Physics Letters A 451 (2022) 128427

Contents lists available at ScienceDirect

Physics Letters A

www.elsevier.com/locate/pla

A simple three-dimensional quadratic flow with an attracting torus

Mahtab Mehrabbeik [a], Sajad Jafari [a,b,*], Julien Clinton Sprott [c]

[a] Department of Biomedical Engineering, Amirkabir University of Technology (Tehran Polytechnic), Tehran, Iran
[b] Health Technology Research Institute, Amirkabir University of Technology (Tehran Polytechnic), Tehran, Iran
[c] Department of Physics, University of Wisconsin, Madison, WI 53706, USA

ARTICLE INFO

Article history:
Received 9 July 2022
Received in revised form 2 September 2022
Accepted 4 September 2022
Available online 13 September 2022
Communicated by M. Perc

Keywords:
Attracting torus
Nosé-Hoover oscillator
Anti-damping term
Basin of attraction
Multistability

ABSTRACT

Attracting torus is a rare phenomenon in the dynamics of low-dimensional autonomous systems. Adding an anti-damping term to the well-known Nosé-Hoover oscillator, this paper introduces a new system exhibiting attracting torus in a wide range of parameter values. This system has a variety of dynamical solutions like limit cycles, strange attractors, attracting tori, invariant tori, and chaotic sea. It is also demonstrated that the system is multistable in some regions of parameter space wherein different types of attractors coexist. However, the attracting torus is the leading bounded solution in a considerable area of parameter space. Moreover, the coexistence of four limit cycles is found in the time-reversed system. The study of the system's basin of attraction shows that the system owns a solid basin of attraction with rounded boundaries for the attracting torus, which is an exciting property.

1. Introduction

Many researchers have decided to propose or design chaotic systems with distinctive or fascinating dynamical properties. Due to the importance of equilibria in analyzing the dynamics of a system, introducing new systems with particular equilibrium point(s) has become a hot topic in designing new systems [1]. In this regard, the existence of stable equilibrium point(s) [2,3], no equilibria [4], line(s) [5], curve(s) [6,7], and plane(s) [8] of equilibria in a system has attracted lots of attention. Such systems triggered two other topics in designing new chaotic systems: systems with hidden attractors and systems with multistability. On the one hand, the systems with hidden attractors have been exciting since they are the counterexamples of the relation between unstable equilibrium points and chaotic attractors [9]. On the other hand, the coexistence of two or more simultaneous attractors for a system is inherently an interesting property, especially when these coexisting attractors are of infinite countable or uncountable numbers. These two typical cases of multistability are respectively known as megastability [10,11] and extreme multistability [12,13].

In addition to designing new systems with unique dynamical characteristics, some systems were developed to describe real-world phenomena [14,15]. Lorenz system [16], Hodgkin-Huxley model [17], and Nosé-Hoover oscillator [18] are three well-known examples of such systems. The Nosé-Hoover oscillator, also known as the Sprott A system, describes the dynamics of a thermostat for a constant temperature. This system is interesting since it has no equilibrium point and two quadrative nonlinearities. Also, the coexistence of an invariant tori with a chaotic sea, which is an unusual property, was observed as its dynamics. Different studies on the Nosé-Hoover system revealed some exciting behaviors of this oscillator, although it is a conservative system. Moreover, in the study on categorizing conservative flows, the Nosé-Hoover system was identified in the third case of conservative flows since numerical solutions (not analytic ones) are needed to prove that this system is conservative [19]. Furthermore, adding a damping term to the Nosé-Hoover equations, a chaotic system with adjustable Kaplan-Yorke dimension (D_{KY}) was reported in [20].

Although finding chaotic dynamics in a nonlinear system is of high importance, observing nonchaotic dynamics, such as attracting torus, is interesting as well. The reason is that attracting torus is a sporadic dynamical behavior that has hardly been observed in low-dimensional autonomous nonlinear systems. Some studies reported the existence of attracting torus in nonautonomous systems. For instance, in [21], the authors showed how adding a forcing term to a simple two-dimensional system can change the system's dynamics from exhibiting the limit cycles to attracting torus and chaos. However, a few studies indicated attracting torus in the three-dimensional autonomous systems. As an illustration, a symmetric coexistence of two attracting tori in a three-dimensional autonomous system was reported in [22].

This paper proposes an anti-damping term for the Nosé-Hoover system, resulting in a three-dimensional dissipative system with

* Corresponding author.
E-mail address: sajadjafari@aut.ac.ir (S. Jafari).

https://doi.org/10.1016/j.physleta.2022.128427
0375-9601/

rich dynamical properties. In the following sections, the system is defined (Section 2), and its dynamical properties, such as the system equilibrium point, its stability analysis, the coexistence of different types of attractors, the monostability region of the attracting torus, bifurcation diagrams, and the dynamical properties of the time-reversed system (Section 3) is described in details. Finally, to conclude the paper, the most important results are summarized (Section 4).

2. System definition

The Nosé-Hoover oscillator is a famous instance of a conservative system that has intensively been investigated. The definition of the Nosé-Hoover oscillator is

$$\begin{aligned}\dot{x} &= y\\ \dot{y} &= -x + yz\\ \dot{z} &= a - y^2\end{aligned} \tag{1}$$

here, yz is the nonlinear damping, which impacts on lowering the difference of y^2 and the parameter a. Considering y^2 as the normalized temperature in each moment, yz plays the role of a thermostat in System (1). Using different sets of initial conditions, the Nosé-Hoover oscillator solutions contain an infinite number of nested tori encircled by a chaotic sea. Generally, for a three-dimensional conservative system, the following condition must be met:

$$Tr(Jac.) = \frac{\partial \dot{x}}{\partial x} + \frac{\partial \dot{y}}{\partial y} + \frac{\partial \dot{z}}{\partial z} = 0 = \lambda_1 + \lambda_2 + \lambda_3 \tag{2}$$

where $Tr(Jac.)$ indicates the trace of the system's Jacobian matrix, and λ_i are the system's Lyapunov exponents (LEs) for a specific attractor. Based on the classification presented in [19], a conservative system can be categorized into four groups. This case, wherein $Tr(Jac.) = -z$ and $\langle z \rangle = 0$, can be categorized in the third case of the conservative flows since the system's local divergence is state-dependent that can not be detected as a conservative solution by a glance at the equations of the system or, in other words, checking the boundedness condition. Note that $\langle . \rangle$ indicates averaging over time. Adding a damping term to the right-hand side equations is the most straightforward way, leading to dissipative solutions. Adding the damping term $-by$ to $\dot{y}$ equation, the system becomes:

$$\begin{aligned}\dot{x} &= y\\ \dot{y} &= -x + yz - by\\ \dot{z} &= a - y^2\end{aligned} \tag{3}$$

where $Tr(Jac.) = z - b$ and b is the control parameter. Assuming $z' = z - b$, System (3) remains the same. Therefore, adding the damping term to $\dot{y}$ equation cannot help to make the system dissipative, and the system remains conservative. On the other hand, the addition of $-bx$ to $\dot{x}$ equation, as the damping term, can discontinuously reduce the D_{KY} by raising the b parameter. Similarly, adding $-bz$ to $\dot{z}$ equation can make the system dissipative, while the regions of chaotic solutions are too restricted. Nevertheless, as mentioned in [20], replacing y^2, which is one of the nonlinearities of the Nosé-Hoover system, by a weaker nonlinear term $|y|$ leads to a continuous decreasing trend of D_{KY} by the increase b value.

Applying $z \to -z$, another version of the Nosé-Hoover oscillator can be defined as:

$$\begin{aligned}\dot{x} &= y\\ \dot{y} &= -x - yz\\ \dot{z} &= y^2 - a\end{aligned} \tag{4}$$

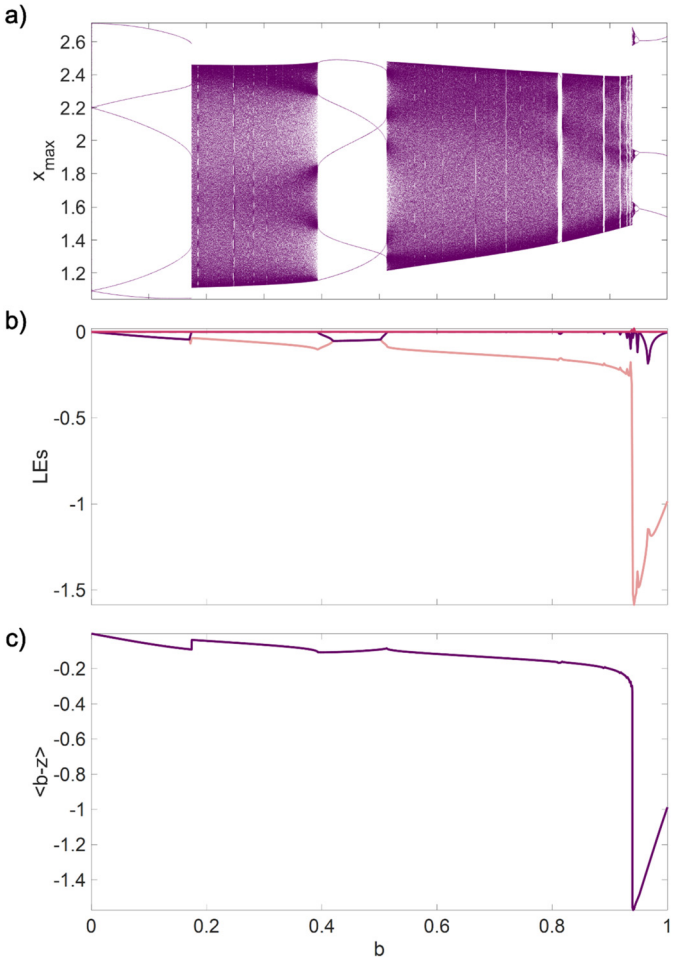

Fig. 1. a) The bifurcation diagram b) LEs spectra, and c) the dissipation diagram of System (5) for $a = 7$ and $0 \leq b \leq 1$. The diagrams are plotted assuming the end of the trajectory obtained for each b value as the initial conditions for the subsequent step calculations. Also, the first initial condition is $(x_0, y_0, z_0) = (0.5, 0.5, 0)$. The figure shows how the system dynamics and dissipativity varies as the value of the parameter b changes.

All the characteristics mentioned for the Nosé-Hoover system can also be found in System (4). Adding an anti-damping term bz to the $\dot{z}$ equation can lead to a dissipative system which can be presented as follows:

$$\begin{aligned}\dot{x} &= y\\ \dot{y} &= -x - yz\\ \dot{z} &= y^2 - a + bz\end{aligned} \tag{5}$$

here, $Tr(Jac.) = b - z$. The parameter b (b is considered a positive real number) is the control parameter. Numerical analysis proves that System (5) is a dissipative system since the $\langle b - z \rangle < 0$ as the value of b parameter gradually grows. It can be seen that the addition of the anti-damping term affects the system's local divergence by adding the term b to the $Tr(Jac.)$. Hence, at first glance, it is expected to have an unbounded solution. However, the anti-damping parameter impacts the system's dynamic so that the system surprisingly can exhibit bounded dissipative solutions. Fig. 1 demonstrates the system's bifurcation diagram versus b parameter, its corresponding LEs spectra (employing the Wolf algorithm [23] with the run-time of 100000 seconds), and dissipation diagram (value of $\langle b - z \rangle$) of System (5) for $a = 7$, $0 < b \leq 1$, and the initial conditions of $(x_0, y_0, z_0) = (0.5, 0.5, 0)$. It should be noted that the initial conditions for obtaining the system's dynamics for

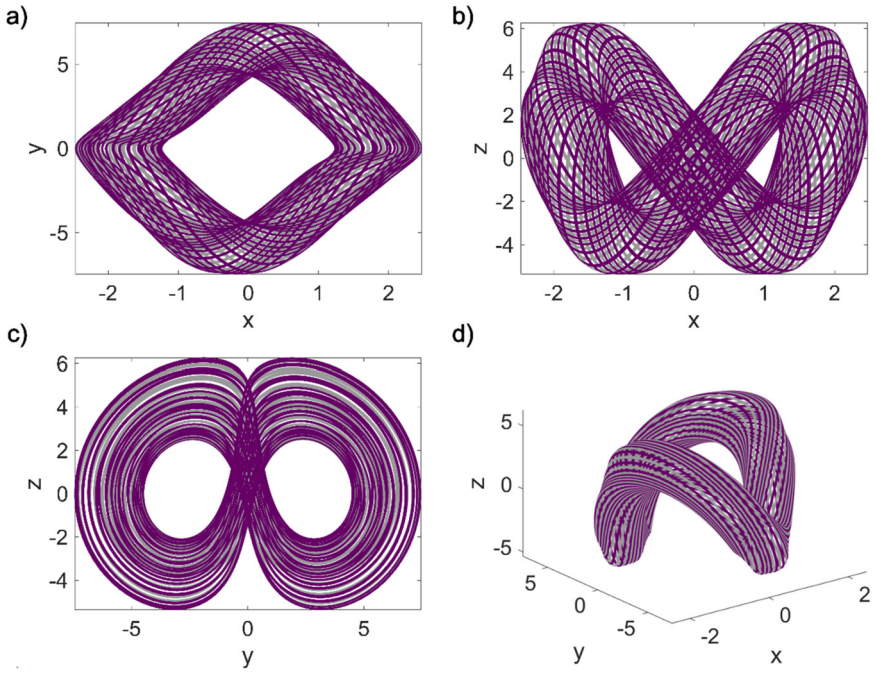

Fig. 2. The attracting torus of System (5) in a) x-y, b) x-z, c) y-z planes and d)x-y-z space considering $a = 7$, $b = 0.55$ and $(x_0, y_0, z_0) = (0.5, 0.5, 0)$. The system owns a fat monostable attracting torus in this set of parameters.

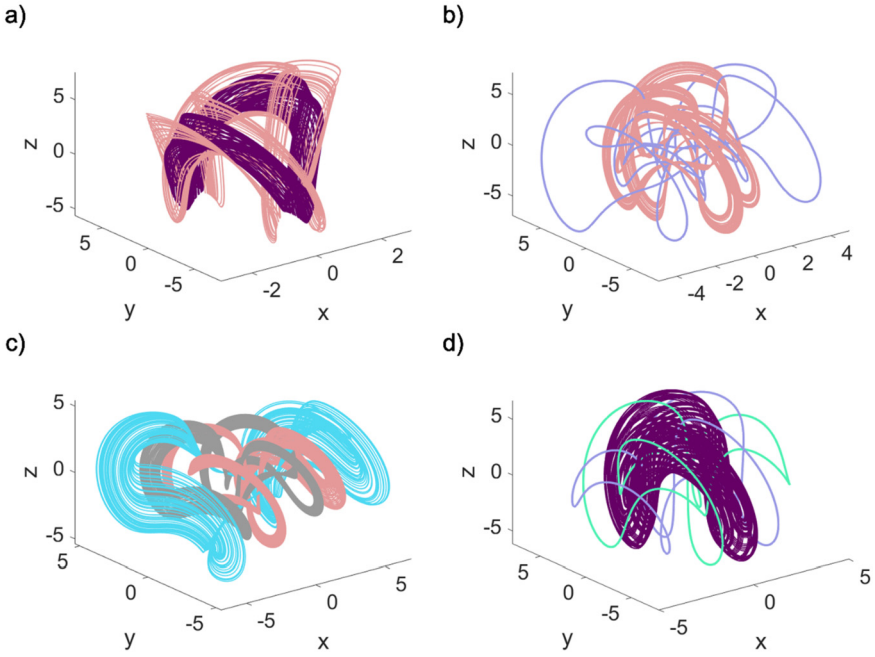

Fig. 3. The coexisting attractors of System (5) in a) $(a, b) = (7, 0.925)$, b) $(a, b) = (2.7804, 0.1192)$, c) $(a, b) = (4.162, 0.1)$, and d) $(a, b) = (7, 0.3)$. Dark purple indicates the attracting torus. Also, the chaotic attractor is presented in light pink, gray, and cyan colors. Light purple and light green also signify the limit cycles. More details can be found in Table 1. The system has rich dynamical properties and shows the exciting coexistence of different attractors. (For interpretation of the colors in the figure(s), the reader is referred to the web version of this article.)

each step (each b value) are acquired from the last sample of the previous step's trajectory (forward method). This method simply helps to follow or remain in an attractor basin of attraction as the bifurcation parameter varies. Consequently, using this method, multistability can be hopefully identified when applied in different directions (increasing or decreasing the value of the bifurcation parameter). Furthermore, the forward method helps to start solving the system from the nearest point to the trajectory in each step. Therefore, the least transient time can be expected, which confirms that the dynamics shown in the bifurcation diagrams are not transients.

It is very interesting and counter-intuitive that the system is conservative for $b = 0$ but dissipative for both positive and negative b. The authors are unaware of such a feature in any known chaotic system.

From Fig. 1a-b, it can be observed that for about $b \in [0.174, 0.392] \cap [0.514, 0.928]$, there exists two zero and one negative LEs. Thus, Fig. 1 reveals that System (5) owns an attracting torus for a significant range of b values. Fig. 1c also shows how the dissipa-

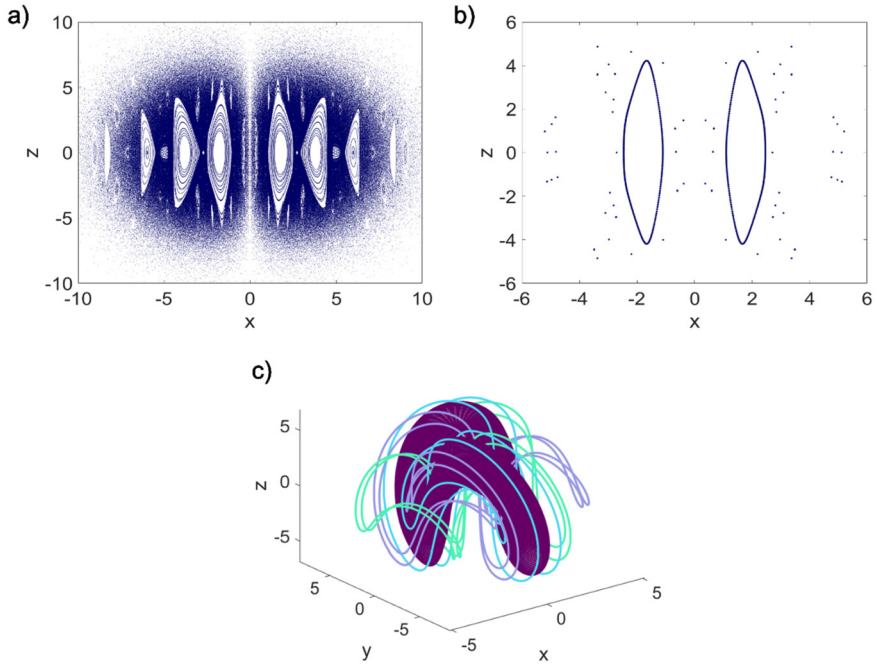

Fig. 4. The cross-section of a) the chaotic sea and nested tori ($(a, b) = (7, 0)$) and b) the attracting torus and limit cycles ($(a, b) = (7, 0.005)$) in the $y = 0$ plane. c) The coexistence of the attracting torus with a pair of period-4 symmetric limit cycles and a period-5 limit cycle (symmetric about the origin) in $(a, b) = (7, 0.005)$. In the absence of the anti-damping term ($b = 0$), the system is the original conservative Nosé-Hoover system. However, even a small strength of the anti-damping term makes the system dissipative. Also, in small values of parameter b, the system shows multistability.

tivity of System (5) varies as the value of parameter b changes. Observing an attracting torus in the dynamics of bounded autonomous systems is exceptionally infrequent. In contrast, attracting torus is typical behavior that can be noticed in nonautonomous megastable systems like the ones reported in [21]. As an example, attracting torus in a three-dimensional autonomous system was previously observed in [22] but in a small range of parameter values. The attracting torus of System (5) is represented in Fig. 2 for $(a, b) = (7, 0.55)$ and $(x_0, y_0, z_0) = (0.5, 0.5, 0)$.

Employing the Wolf algorithm [23], the LEs of the fat attracting torus, represented in Fig. 2, are $(\lambda_1, \lambda_2, \lambda_3) = (0, 0, -0.1041)$ with the run-time of 100000 seconds.

3. Dynamical characteristics

The Nosé-Hoover system defined in Eq. (4) is originally a no-equilibrium system. For a system to have an equilibrium point, there must be at least one set of (x^*, y^*, z^*) value which makes the right-hand side system's equations zero. Accordingly, setting $y = 0$, $-x - yz = 0$, and $y^2 - a + bz = 0$, the only equilibrium point of System (5) is $(x^*, y^*, z^*) = (0, 0, \frac{a}{b})$. The eigenvalues of this equilibrium satisfy the following condition:

$$\lambda^3 - f_3\lambda^2 - f_2\lambda - f_1 = 0 \tag{6}$$

where $f_3 = \frac{1}{b}(a - b^2)$, $f_2 = a - 1$, and $f_1 = b$. Applying the Routh–Hurwitz criterion, the system's equilibrium point is stable for $f_3 < 0$, $f_1 < 0$, and $f_2 f_3 + f_1 > 0$ or, in other words, $\frac{1}{b}(a - b^2) < 0$, $b < 0$, and $\frac{1}{b}(a - b^2)(a - 1) + b > 0$. Since one eigenvalue is the parameter b, the system's equilibrium point is never stable for $b \geq 0$. Also, it appears that for $a > 2b$ the equilibrium point is a saddle-node. Note that the unstable manifold is z axis and the other two manifolds are in the $z = 0$ plane. Looking more closely at the stability criteria, for $b < 0$, the stability of the equilibrium point depends on the sign of the parameter a. More specifically, for $b, a < 0$, the equilibrium point is stabled, otherwise, i.e., for $b < 0$ and $a > 0$, the system has a saddle-node equilibrium point.

Furthermore, applying $(x, y, z) \to (-x, -y, z)$, the system remains unaffected. So, System (5) is symmetric with respect to the z axis.

3.1. Multistability

Performing an extensive numerical search in the two-dimensional parameter space of (a, b) where $a \in [0, 20]$ and $b \in [0, 1]$, reveals that System (5) has rich dynamical properties, and the exciting coexistence of different attractors can be observed for various values of a and b parameters. Fig. 3a shows the coexistence of an attracting torus (dark purple) and a chaotic attractor (light pink). The coexistence of a strange attractor (light pink) and a period-5 limit cycle (light purple) is also demonstrated in Fig. 3b. In Fig. 3c, a symmetric pair of chaotic attractors (light pink and gray) surrounded by another chaotic coexisting attractor (cyan) can be observed. Similarly, Fig. 3d illustrates the coexistence of a symmetric pair of period-2 limit cycles (light purple and light green) with an attracting torus (dark purple). More details, such as initial conditions, LEs, D_{KY}, and parameter values are given in Table 1.

Apparently, when $b = 0$, System (5) becomes a conservative system owning nested conservative tori and a chaotic sea. The Poincaré section of these nested tori within the chaotic sea is represented in Fig. 4a. According to Fig. 4b, as soon as the value of b parameter slightly increases, the system becomes dissipative, and an attracting torus appears in coexistence with three limit cycles, including a pair of symmetric period-4 limit cycles and a period-5 limit cycle symmetric about the origin, shown in Fig. 4c.

3.2. Bifurcations and dynamics region

It is observed that in $a = 7$ and $b = 0.3$, System (5) has three coexisting attractors, including an attracting torus and a pair of symmetric limit cycles. Considering three initial conditions of $(x_{01}, y_{01}, z_{01}) = (0.5, 0.5, 0)$, $(x_{02}, y_{02}, z_{02}) = (2.5, -8, 0)$, and $(x_{03}, y_{03}, z_{03}) = (-2.5, 8, 0)$, that respectively lead to the attracting torus and limit cycles, the bifurcation diagram of System (5) is

Table 1
The details of attractors that are presented in Fig. 3. The considered run-time for calculating the LEs is 1000000 seconds.

Fig.	(a, b)	(x_0, y_0, z_0)	$(\lambda_1, \lambda_2, \lambda_3)$	D_{KY}	Attractor type	Color
3a	$(7, 0.925)$	$(1.5, 0, 1.6)$	$(0, 0, -0.2356)$	2.0	Attracting torus	Dark purple
		$(1.9, 0, 0.7)$	$(0.0625, 0, -1.7425)$	2.0359	Strange attractor	Light pink
3b	$(4.162, 0.1)$	$(3, 0, 0.5)$	$(0.0231, 0, -0.0981)$	2.2355	Strange attractor	Light pink
		$(6, 0, 0.8)$	$(0, -0.0425, -0.0425)$	1.0	Limit cycle	Light purple
3c	$(2.7804, 0.1192)$	$(\pm 9.14, 0, 2.7)$	$(0.0348, 0, -0.1514)$	2.2299	Symmetric pair of strange attractors	Light pink/gray
		$(-9.7, 0, 7.6)$	$(0.0348, 0, -0.1517)$	2.2294	Strange attractor	cyan
3d	$(7, 0.3)$	$(0.5, 0.5, 0)$	$(0, 0, -0.0637)$	2.0	Attracting torus	Dark purple
		$(\pm 2.5, \mp 8, 0)$	$(0, -0.0214, -0.0214)$	(1.0)	Symmetric pair of limit cycles	Light purple/light green

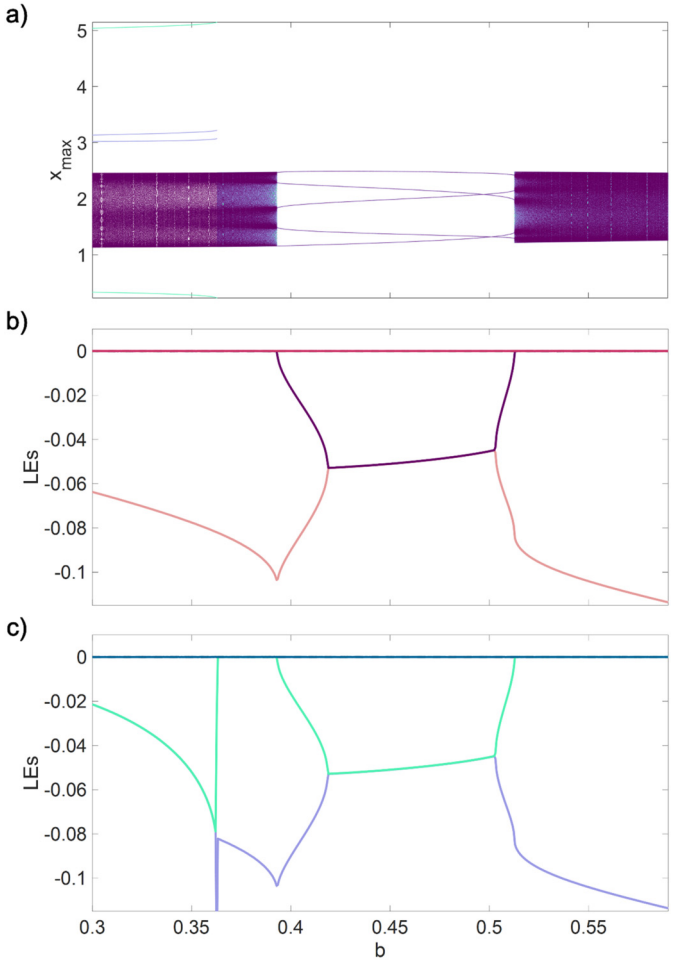

Fig. 5. a) The bifurcation diagrams and b, c) LEs spectra of System (5) for $a = 7$ and $0.3 \leq b \leq 0.59$, using the forward method. The first initial conditions are $(x_{01}, y_{01}, z_{01}) = (0.5, 0.5, 0)$, $(x_{02}, y_{02}, z_{02}) = (2.5, -8, 0)$, and $(x_{03}, y_{03}, z_{03}) = (-2.5, 8, 0)$ that respectively lead to the attracting torus and symmetric limit cycles in $(a, b) = (7, 0.3)$. In $b \in [0.3, 0.363)$ the attracting torus coexists with a pair of symmetric period-2 limit cycles. In $b \in (0.393, 0.513)$ the period-5 limit-cycle is supposed to be monostable. Also, in $b \in [0.363, 0.393] \cap [0.513, 0.59]$ the attracting torus is conceivable to be monostable.

plotted in Fig. 5a for $a = 7$ and $0.3 \leq b \leq 0.59$, using the forward method. Also, employing the Wolf algorithm [23] with the run-time of 100000 seconds, the LEs of System (5) are also calculated. Fig. 5b shows the LEs spectra of System (5), which correspond to the dark purple bifurcation (attracting torus). Similarly, Fig. 5c shows the LEs spectra for the symmetric limit cycles.

From Fig. 5, it can be seen that the limit cycles collide with the attracting torus through a boundary crisis at about $b = 0.363$. After the boundary crisis at about $b = 0.393$, though which the attracting torus annihilated, a large periodic window occurs in $b \in (0.393, 0.513)$. Likewise, through a boundary crisis at $b = 0.513$, the attracting torus appears.

Fig. 5 can be divided into three regions: The region of coexistence of attracting torus and the symmetric pair of period-2 limit cycles ($b \in [0.3, 0.363)$), the suspectable region of monostability of period-5 limit cycle ($b \in (0.393, 0.513)$), and the potential region of monostability of the attracting torus ($b \in [0.363, 0.393] \cap [0.513, 0.59]$). Hence, there are two separate areas wherein the attracting torus can be monostable. It is found that in some regions of $b \in [0.3, 0.363)$, there exists another period-3 limit cycle that coexists with the stated period-5 limit cycle. On the other hand, the results approve that the attracting torus is monostable for $b \in [0.363, 0.393] \cap [0.513, 0.59]$. It should be mentioned that the numerical search results indicate that the attracting torus vanishes as soon as parameter a reaches about 8.5 for any values of b parameter.

Fig. 6a shows the basins of attraction for System (5) in three $y = 0$, $z = 0$, and $x = 0$ planes. A solid basin of attraction can be observed as b parameter is selected in $0.363 \leq b < 0.513$. However, as illustrated in Fig. 6b, when b parameter is selected in $[0.513, 0.59]$, filamentary unbounded regions, spread through the system's basin of attraction, can be noticed. Also, the basin of attraction gets more limited by increasing the b parameter value. The bifurcation diagrams presented in Fig. 5a are plotted for $0.3 \leq b \leq 0.59$ since for $b > 0.59$, the solution gets unstable due to these scattered unbounded regions within the torus basin of attraction. Figs. 6c-e show how the torus basin of attraction shrinks by growing b values up to 0.9.

3.3. Time-reversed system

According to Fig. 6a, it can be observed that System (5) is monostable for $(a, b) = (7, 0.37)$ and the attracting torus is the only attractor of the system. Hence it is interesting to study the dynamics of the time-reversed system to check whether the attracting torus exists in the time-reversed version of the system. Setting $(a, b) = (7, 0.37)$ and applying $t \to -t$, the time-reversed version of System (5) can be achieved as:

$$\begin{aligned} \dot{x} &= -y \\ \dot{y} &= x + yz \\ \dot{z} &= a - y^2 - bz \end{aligned} \tag{7}$$

The results of a comprehensive numerical search reveal that System (7) has four coexisting period-1 limit cycles for $a = 7$ and $b = 0.37$, which are shown in Fig. 7. Moreover, Fig. 8 presents the basins of attractions for System (7) in $z = 0$, $y = 0$, and $x = 0$ planes. The basin of attraction of each limit cycle in Fig. 7 is represented with the same color, used to plot their trajectories.

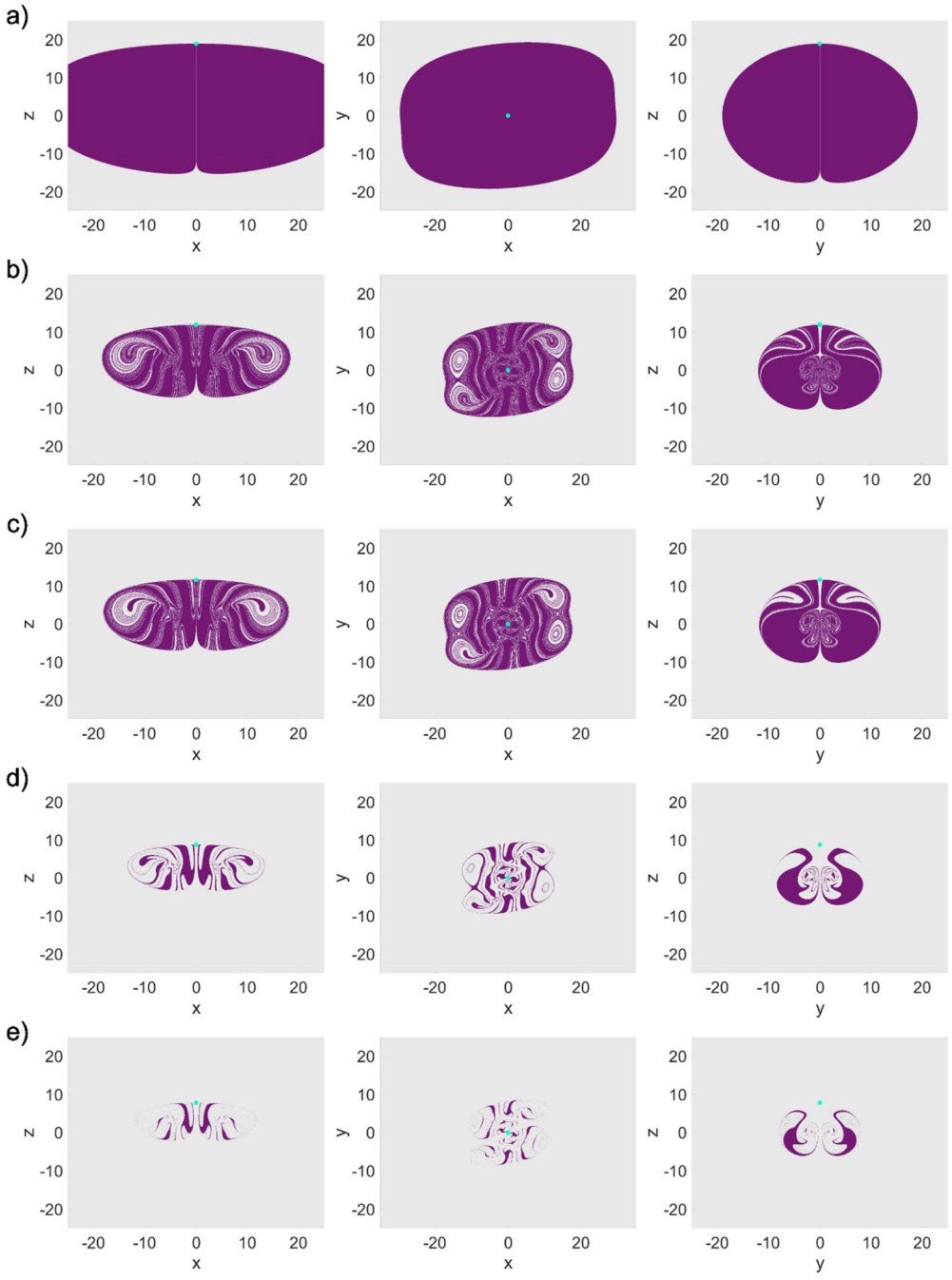

Fig. 6. The basins of attraction of System (5) for $a = 7$ and a) $b = 0.37$, b) $b = 0.59$, c) $b = 0.6$, d) $b = 0.8$, and e) $b = 0.9$ in $y = 0$ (left panel), $z = 0$ (middle panel), and $x = 0$ (right panels) planes. Dark purple, light gray, and light green colors respectively indicate the attracting torus, the unbounded orbits, and the unstable equilibrium. The figure portrays how the basin of attraction of the attracting torus in its monostability region shrinks by growing the value of the parameter b.

Interestingly, no regions of scattered unbounded orbits can be found in Fig. 8 (in contrast to Fig. 6a). The results show that, unlike the original system, the time-reversed system does not have a variety of different dynamical solutions, and no other types of attractors are detected for it.

4. Conclusion

Adding an anti-damping term to the third equation of the Nosé-Hoover system, this paper described the exciting and rare characteristics of the three-dimensional quadratic system based on the Nosé-Hoover oscillator. An intriguing property of this system is that, depending on parameters, it has different dynamical solutions like limit cycles, attracting torus, and strange attractor, as well as invariant tori and a chaotic sea (for $b = 0$). Despite the nonautonomous megastable systems, attracting torus is an incredibly rare dynamic for autonomous systems. Previously, the coexistence of two symmetric attracting tori was found in a three-dimensional system introduced in [22]. However, in this case, the coexistence of an attracting torus with a strange attractor and also with a symmetric pair of limit cycles was found. Moreover, the coexistence of three chaotic attractors (two symmetric with another strange attractor) and a strange attractor with a period-5 limit cycle was observed. Some regions of parameters were found in which the attracting torus was the only dynamical solution of the system. The study of the system basins attraction showed a solid region with

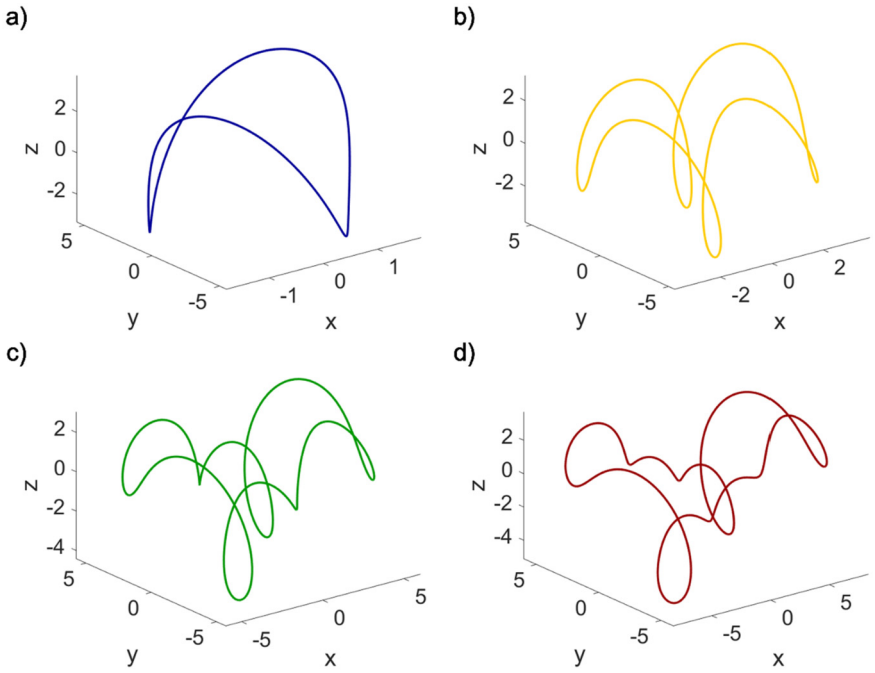

Fig. 7. The coexisting period-1 limit cycles of System (7) for $a = 7$ and $b = 0.37$ using the initial condition of a) $(x_{01}, y_{01}, z_{01}) = (0, 5, 0)$, b) $(x_{02}, y_{02}, z_{02}) = (0.5, 0.5, 0)$, c) $(x_{03}, y_{03}, z_{03}) = (1, 1, 1)$, and d) $(x_{04}, y_{04}, z_{04}) = (-8.5, 0, -1)$. The time-reversed system has four coexisting period-1 limit cycles in a parameter set wherein the original system exhibits a monostable attracting torus.

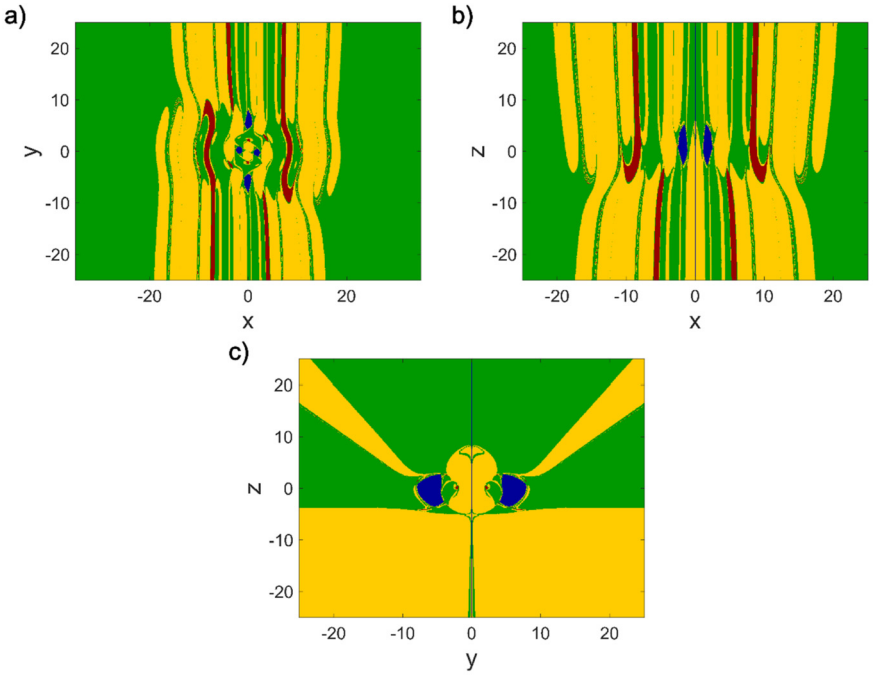

Fig. 8. The basins of attraction of System (7) for $a = 7$ and $b = 0.37$ in a) $z = 0$, b) $y = 0$, and c) $x = 0$ planes. Yellow, green, dark red, and dark blue colors indicate the limit cycles in Fig. 7 with the same colors, respectively. No regions of scattered unbounded orbits can be observed in the basin of attraction of the time-reversed system.

clear rounded boundaries for the attracting torus' basin of attraction when $b \in [0.363, 0.393]$. In contrast, when b is selected in $[0.513, 0.59]$ range, scattered unbounded orbits were seen within the torus' basin of attraction which was shrunk as b gradually grew.

The study of the time-reversed system showed that four period-1 limit cycles coexisted in the same parameter set where the original system exhibited a monostable attraction torus with a solid rounded basin of attraction. Moreover, no unbounded orbits were detected in the basin of attraction of the system in such parameter sets.

CRediT authorship contribution statement

Mahtab Mehrabbeik: Writing – original draft, Software, Methodology, Investigation. **Sajad Jafari:** Writing – review & editing, Supervision, Conceptualization. **Julien Clinton Sprott:** Writing – review & editing, Supervision, Project administration, Methodology, Conceptualization.

Declaration of competing interest

The authors declare that they have no known competing financial interests or personal relationships that could have appeared to influence the work reported in this paper.

Data availability

No data was used for the research described in the article.

References

[1] Z. Wanget, et al., Chaotic flows with special equilibria, Eur. Phys. J. Spec. Top. 229 (6) (2020) 905–919.
[2] Q. Li, H. Zeng, J. Li, Hyperchaos in a 4D memristive circuit with infinitely many stable equilibria, Nonlinear Dyn. 79 (4) (2015) 2295–2308.
[3] M. Chen, C. Wang, H. Bao, X. Ren, B. Bao, Q. Xu, Reconstitution for interpreting hidden dynamics with stable equilibrium point, Chaos Solitons Fractals 140 (2020) 110188.
[4] Z. Wei, Dynamical behaviors of a chaotic system with no equilibria, Phys. Lett. A 376 (2) (2011) 102–108.
[5] H. Bao, N. Wang, B. Bao, M. Chen, P. Jin, G. Wang, Initial condition-dependent dynamics and transient period in memristor-based hypogenetic jerk system with four line equilibria, Commun. Nonlinear Sci. Numer. Simul. 57 (2018) 264–275.
[6] T. Gotthans, J. Petržela, New class of chaotic systems with circular equilibrium, Nonlinear Dyn. 81 (3) (2015) 1143–1149.
[7] Y. Chen, Q. Yang, A new Lorenz-type hyperchaotic system with a curve of equilibria, Math. Comput. Simul. 112 (2015) 40–55.
[8] J. Petrzela, T. Gotthans, New chaotic dynamical system with a conic-shaped equilibrium located on the plane structure, Appl. Sci. 7 (10) (2017) 976.
[9] S. Nag Chowdhury, D. Ghosh, Hidden attractors: a new chaotic system without equilibria, Eur. Phys. J. Spec. Top. 229 (6) (2020) 1299–1308.
[10] P. Prakash, K. Rajagopal, J. Singh, B. Roy, Megastability in a quasi-periodically forced system exhibiting multistability, quasi-periodic behaviour, and its analogue circuit simulation, AEÜ, Int. J. Electron. Commun. 92 (2018) 111–115.
[11] Y. Tang, H.R. Abdolmohammadi, A.J.M. Khalaf, Y. Tian, T. Kapitaniak, Carpet oscillator: a new megastable nonlinear oscillator with infinite islands of self-excited and hidden attractors, Pramana 91 (1) (2018) 11.
[12] Q. Wan, Z. Zhou, W. Ji, C. Wang, F. Yu, Dynamic analysis and circuit realization of a novel no-equilibrium 5D memristive hyperchaotic system with hidden extreme multistability, Complexity 2020 (2020).
[13] Y. Zhang, Z. Liu, H. Wu, S. Chen, B. Bao, Two-memristor-based chaotic system and its extreme multistability reconstitution via dimensionality reduction analysis, Chaos Solitons Fractals 127 (2019) 354–363.
[14] S. Khajanchi, M. Perc, D. Ghosh, The influence of time delay in a chaotic cancer model, Chaos, Interdiscip. J. Nonlinear Sci. 28 (10) (2018) 103101.
[15] J.-M. Ginouxet, et al., Is type 1 diabetes a chaotic phenomenon?, Chaos Solitons Fractals 111 (2018) 198–205.
[16] E.N. Lorenz, Deterministic nonperiodic flow, J. Atmos. Sci. 20 (2) (1963) 130–141.
[17] A.L. Hodgkin, A.F. Huxley, A quantitative description of membrane current and its application to conduction and excitation in nerve, J. Physiol. 117 (4) (1952) 500.
[18] W.G. Hoover, Canonical dynamics: equilibrium phase-space distributions, Phys. Rev. A 31 (3) (1985) 1695.
[19] S. Jafari, J.C. Sprott, S. Dehghan, Categories of conservative flows, Int. J. Bifurc. Chaos 29 (02) (2019) 1950021.
[20] B. Munmuangsaen, J.C. Sprott, W.J.-C. Thio, A. Buscarino, L. Fortuna, A simple chaotic flow with a continuously adjustable attractor dimension, Int. J. Bifurc. Chaos 25 (12) (2015) 1530036.
[21] Z. Wang, H.R. Abdolmohammadi, F.E. Alsaadi, T. Hayat, V.-T. Pham, A new oscillator with infinite coexisting asymmetric attractors, Chaos Solitons Fractals 110 (2018) 252–258.
[22] J. Sprott, S. Jafari, V.-T. Pham, Z.S. Hosseini, A chaotic system with a single unstable node, Phys. Lett. A 379 (36) (2015) 2030–2036.
[23] A. Wolf, J.B. Swift, H.L. Swinney, J.A. Vastano, Determining Lyapunov exponents from a time series, Phys. D: Nonlinear Phenom. 16 (3) (1985) 285–317.